Journal of Medicines Development Sciences, 2022, Volume 7, Issue 1
https://ojs.whioce.com/index.php/jmds/index
ISSN Online: 2382-6371
ISSN Print: 2382-6363

Understanding the Habitual Pattern of Concomitant Consumption of Herbs to Alleviate the Symptoms of Ulcerative Colitis by Comparative Proteome Analysis

Songhua Deng[1,2]*, Hairong Long[1,2], Duolin Wu[1,2], Zhenqiu Xiao[1,2], Sai Chen[2], Chunju He[2], Zuqing Yang[2]

[1]Surgery of Traditional Chinese Medicine, Guangxi University of Traditional Chinese Medicine, Nanning 530001, Guangxi Province, China

[2]Surgical Department, Guangxi International Zhuang Medical Hospital, Nanning 530001, Guangxi Province, China

***Corresponding author:** Songhua Deng, dsh198065@163.com

Abstract: Anchang decoction is an empirical prescription for the treatment of ulcerative colitis in China. In order to better understand its therapeutic function, large efforts have been made to identify its chemical constituents and to unravel the efficacy of its principal constituents. However, the molecular mechanism of its combinations is still unclear. Proteomics application has yielded some positive results in drug development and the identification of potential drug targets, suggesting the potential of this analytical approach to explore the action of molecular mechanisms of herbal formula by robustly addressing dynamic proteome changes. Label-free quantification and parallel reaction monitoring were used to identify differentially expressed proteins in the colon tissue of ulcerative colitis rats, fed with Anchang decoction and mesalazine, respectively. In this study, a total of 1,182 proteins were identified. From GO and KEGG analyses, the proteins of cytoskeleton and cytochrome P450 changed significantly with the occurrence of ulcerative colitis. In the meantime, antigen binding proteins and antioxidant-related proteins turned out to have drastic fluctuations with mesalazine and Anchang decoction. It has also been confirmed that KRT8, MYH11, FLNA, and LMNA are all related to the formation of ulcerative colitis based on parallel reaction monitoring analysis. The increase in FGG in the ulcerative colitis rat model is due to mesalazine, whereas that in KRT8 is due to Anchang decoction. The results from this study provide insights for the mechanism of action of Anchang decoction, which turns out to be an efficient technical pipeline for understanding worldwide medicinal herbs.

Keywords: Traditional Chinese medicine; Ulcerative colitis; Proteomics; Parallel reaction monitoring; Mechanism of action

Online publication: July 29, 2022

1. Introduction

With the changes of diet and living habits, the number of patients with ulcerative colitis (UC) is increasing all over the world. UC is a subclass of inflammatory bowel disease (IBD), and it is caused by an intestinal antigen immune disorder in genetically susceptible hosts [1]. UC is a chronic disease with clinical manifestations of dysentery, rectal irritation, and abdominal pain [2]. UC is caused by epithelial cell or structural dysfunction and an inflammatory cascade triggered by inflammatory mediators and cells in the lamina propria. Therefore, therapeutic strategies should target epithelial cells or inflammatory cells to

restore intestinal barrier function and achieve remission [3]. Currently, mesalazine (5-aminosalicylic acid) is the most common therapeutic drug used to treat UC. However, 30-45% of patients taking mesalazine still experienced the recurrence of symptoms [4], accompanied by side effects, such as aggravation of UC, gastrointestinal symptoms, pancreatitis, hepatotoxicity, and nephrotoxicity [5]. Therefore, more effective alternatives are required.

Anchang decoction (ACD) is a well-known empirical prescription in Guangxi, and it has been used to treat UC patients since 1990. ACD can improve the structural deconstruction of epithelial cells in UC patients [6] and enhance their immune function by regulating immunoglobulin IgA, IgG, and IgM [7]. ACD can also lower adenine, cytosine, uridine, lactate, glycine, and glucose, and raise mannose, xylose, sarcosine, and β-alanine, which help to regulate the intestinal microecology in UC mice. Its effect was found to be better than mesalazine [8]. In addition, ACD may play a role in the prevention and treatment of UC patients by regulating the IL-6/JAK2/STAT3/SOCS-3 signaling pathway [9]. Previous studies have preliminarily revealed the action of ACD in the treatment of UC, but the target and specific mechanism of action are still unclear. This is not conducive to the development and utilization of traditional medicine.

Proteins are the performers of life functions. Using proteomics to gain insight into the molecular mechanisms by which herbal medicines are effective in treating UC [10] has gained much attention from research circles. Therefore, in this study, a UC model was established in rats, and they were fed with mesalazine and ACD, followed by a proteomic analysis of colonic tissues in an attempt to identify the molecular mechanisms underlying the alleviating effect of ACD on UC.

2. Materials and methods

2.1. Materials

ACD was purchased from the First Affiliated Hospital of Guangxi University of Traditional Chinese Medicine. The medicinal components of ACD include 25 grams of psoralen, 20 grams of Astragalus, 15 grams of areca, 15 grams of Codonopsis pilosula, 15 grams of cooked aconite, 15 grams of Poria cocos, 15 grams of Pulsatilla, 15 grams of red peony, 15 grams of Sanguisorba officinalis, 10 grams of dried ginger, 10 grams of wood incense, 10 grams of Atractylodes macrocephala, 10 grams of chicken's inner gold, 10 grams of Xuanhusuo, 10 grams of coix seed, and 10 grams of licorice. Mesalazine was purchased from Sunflower Pharmaceutical Group (Shenzhen, China). 2,4,6-trinitrobenzene sulfonic acid (TNBS) was purchased from Toppon Biotechnology Co., Ltd. (Nanning, China). Trypsin, phenylmethanesulfonyl fluoride (PMSF), and Bradford protein assay kit were purchased from Beyotime Biotechnology (Shanghai, China), while dithiothreitol (DTT) was purchased from Aladdin (Shanghai, China).

2.2. Animal experiment

2.2.1. Animal

Sprague-Dawley rats (220 ± 20 g) were provided by the Experimental Animal Center of Guangxi Medical University (Certificate of Conformity number: SCXK 2014-20002). All animal experimental procedures were performed in accordance with the Guide for the Care and Use of Laboratory Animals, and the experiments were approved by the Animal Ethics Committee of Guangxi University of Traditional Chinese Medicine.

2.2.2. TNBS-induced colitis and berberine treatment

The rats were fed adaptively for one week. During the 12:12 h light-dark cycle, all rats maintained constant humidity (55 ± 5%) and room temperature. The TNBS method was used to induce UC in twelve rats. In short, UC was induced by intrarectal administration of 30 mg of TNBS to each rat, with a total volume of 800 μL (50% ethanol in NaCl/Pi), colitis was induced at 8 cm from the anus by chloral hydrate (mg/kg by

intraperitoneal injection) [11]. After three days, all rats developed UC, and they were then randomly divided into four groups with three rats in each group. From the fourth day onwards, during the induction of colitis, UC rats were given low dose ACD (3.97 g/kg), high dose ACD (19.85 g/kg), and mesalazine (0.42g/kg) daily, which were recorded as ACD-L group, ACD-H group, and mesalazine group, respectively. The remaining group was fed with the same amount of normal saline and recorded as the model group. The other three normal rats were recorded as blank group. After two weeks, the rats were killed 24 hours after the last administration. Intestinal samples from the anus to the ileocecal region were excised. All biological samples were processed and stored at -80℃ for subsequent proteome and pathological analyses. The colon tissue was treated with hematoxylin and eosin (H&E) stains to observe the colon injury.

2.3. Protein extraction, alkylation, and trypsin digestion

The colon tissues were grounded into powder in liquid nitrogen. The powder was added to 300 μL of lysis buffer (8 M urea, 2 mM EDTA, 10 mM DTT, 1% PMSF) and homogenized thoroughly with a tissue grinder. After centrifugation at 4°C and 13,000 × g for 10 minutes, the fragments were removed, and the protein in the supernatant was precipitated with cold acetone solution at -20°C for one to two hours. After centrifugation (12,000 g, 4°C), the protein pellets were collected and redissolved with urea buffer (8 M urea, 100 mm TEAB). The protein concentration was determined according to the instructions found on the Bradford protein assay kit.

100 μg protein from each sample was digested enzymatically as previously described [12]. In short, 10 mM DTT was added at 37℃ for reduction for 30 minutes, and then 25 mM iodoacetamide (IAM) was added for incubation at room temperature for 15 minutes in darkness. 100 mM tetraethylammonium bromide (TEAB) was added to dilute the urea concentration to less than 2 M. Finally, the sample was digested with trypsin (enzyme and substrate 1:50) at 37℃ overnight, and the second digestion (enzyme and substrate 1:100) was carried out over 4 hours, in order to ensure complete cleavage of the sample. After trypsin digestion, salt was removed by Strata-X SPE column, vacuum freeze-dried, and stored at -20℃.

2.4. HPLC fractionation and LC-MS/MS analysis

The dried peptides were reconstituted with HPLC solution A (2% ACN, pH 10) and then fractionated by LC-15AC chromatograph equipped with high pH C18RP column (Bridge Peptide BEH C18, 130Å 3.5 um 4.6*250 mm, Waters). The separation of high pH was carried out by linear gradient with a flow rate of 0.7 mL/min; 0-5 minutes, 0% B (buffer B: 98% acetonitrile, pH = 10); 5-55 minutes, 0-30% B; 55-67 minutes, 30%-100% B; 67-75 minutes, 100% B; 75-78 minutes, 100%-0% B; 78-88 minutes, 100% A (buffer A: 2% acetonitrile, pH = 10). Twelve peptide efflux components were collected from each sample. After vacuum drying, they were combined into four components.

Each component sample was dissolved in 20 μL of 2% acetonitrile, 1 μL was injected, and then Q Exactive HF MS was entered for identification through gradient elution of analytical column. The samples were analyzed using the UltiMate 3000 Nano Upgraded HPLC System equipped with Acclaim PepMap® 100 C18, 3 μm, 100Å (75 μm × 2 cm) trap column and Acclaim PepMap® RSLC C18, 2 μm, 100Å (50 μm × 15 cm) analytical column. The liquid flow rate was 300 nl/min; 0-10 minutes, 5% (buffer B: 0% acetonitrile, 0.1% FA); 10-70 minutes, 50-45% B; 70-73 minutes, 45-90% B; 73-78 minutes, 90% B; 78-78.1 minutes, 90%-5% B; 78.1-90 minutes, 5% B. The eluent was sprayed via NSI source at the 2.5 kV electrospray voltage, and then analyzed by MS/MS in Q Exactive HF. The mass spectrometer was operated in data-dependent mode. Analyzer: Orbitrap; Scan Type: Full; Resolution: 60000; Polarity: +; Scan Range: 400-2000 m/z. Analyzer: Orbitrap; Resolution: 15000; Dynamic Exclusion: 30 s; Charge state: Reject 1; Current Scan Event: Top 15 peaks; Activation Type: HCD; Normalized Collision Energy: 27.

2.5. MS data analysis

The MS data raw file was retrieved from the database using MaxQuan search engine (v.1.6.10.43, https://maxquant.org/) to obtain highly reliable qualitative results. The proteome database of rats (https://www.uniprot.org/proteomes/UP000002494) was used to search the database. The retrieval parameter settings were as follows: trypsin/P was used for digestion; the number of missing digestion sites was set to two; and the minimum length of the peptide segment was set to seven amino acids; the maximum number of modifications of the peptide segment was set to five; the mass error tolerance of the primary parent ion of the first search and main search was set to 20 and 4.5 ppm, respectively; the mass error tolerance was 20 ppm; cysteine alkylation was set as a fixed modification; oxidation on Met was specified as a variable modification; the quantitative method was set to LFQ, and the false discovery rate for protein identification and PSM identification was set to 1%.

2.6. Bioinformatics analysis

Bioinformatics analysis includes functional annotation and differential analysis. Function annotation includes GO (gene ontology) and KEGG (Kyoto Encyclopedia of genes and genes) analysis. GO can be divided into biological process (BP), cellular component (CP), and molecular function (MF). The GO annotation information was mainly obtained from Uniprot-GOA database (http://www.ebi.ac.uk/GOA/). The ID of the protein was first converted into the ID of Uniprot-GOA database. Then, the GO annotation information was found according to this ID. The KEGG online service tool KAAS was used to annotate the protein to obtain the KO number corresponding to the KEGG database. Then, KEGG mapper was used to map the KO number to a specific metabolic pathway. The t-test function in R language was used to calculate the p value between samples. The protein with difference multiple ≥ 1.2 and p value ≤ 0.05 was selected as the difference protein.

2.7. Functional enrichment and functional clustering

GO functional enrichment analysis of differentially expressed proteins (DEPs) using DAVID (https://david-d.Ncifcrf.Gov/) was carried out for enrichment analysis [13]. Fisher's exact test was used in the GO and KEGG analysis of DEPs. Generally, when p value ≤ 0.05, it is considered that this GO function is significantly enriched. The functional cluster analysis of DEPs was analyzed by pheatmap.

2.8. Parallel reaction monitoring analysis

Targeted parallel reaction monitoring (PRM) [14] was used to verify the reliability of the label-based proteomics. An additional 12 rats were selected and divided into four groups. After UC modeling, the three groups were treated in the same manner as 2.3. The UC model rat group was recorded as M, the UC model rats fed with mesalazine were recorded as E, and the UC model rats fed with ACD were recorded as A. The other group of normal rats was recorded as K. Proteins were then extracted from the colon tissues, and 11 DEPs were selected. For PRM analysis, all raw data from PRM experiments and the peptide library were imported into Skyline [15] for processing. In order to ensure high-quality peak detection and integration, manual inspection was performed for further peptide filtration. The unlabeled colon peptide library was used to select peptides and transitions for PRM method development. The PRM signal of each peptide with a high correlation between retention time and dot product compared with the library was included in the analysis. The peptide intensity, reported by summing the peak area of all transitions, was normalized against the BG signal and used for protein comparisons.

3. Results

3.1. Establishment of UC model

Histological analysis revealed the effects of mesalazine and ACD on TNBS-induced UC rats (**Figure 1**). The colonic tissue structure of normal rats (**Figure 1**, Blank) was complete, and there were no pathological changes of fibrous connective tissue proliferation and inflammatory cell infiltration in the submucosa and lamina propria. The UC rats (**Figure 1**, Model) showed significant histological injury when compared with healthy mice. Some inflammatory cell infiltration appeared in the submucosa, suggesting that there was inflammatory reaction in the model rats' colon. After two weeks of administration, compared with the TNBS-induced UC rats, the improvement of ACD-treated (**Figure 1**, ACD-L and ACD-H) and mesalazine-treated rats (**Figure 1**, mesalazine) was obvious, and the infiltration of inflammatory cells in the mucosa and submucosa decreased.

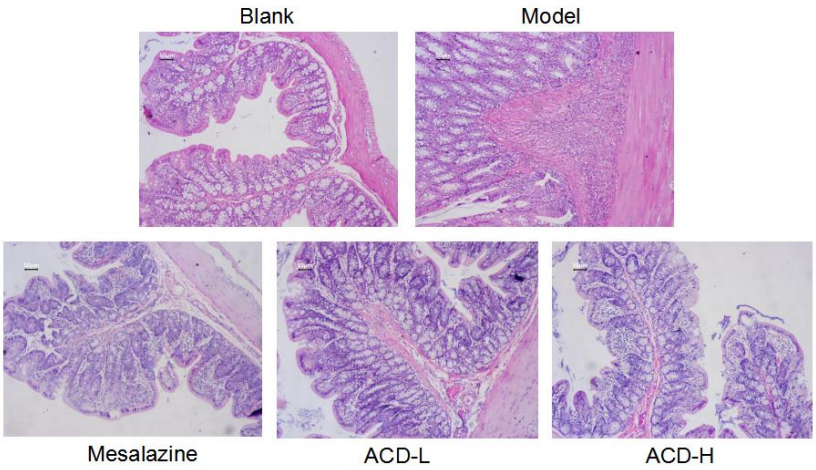

Figure 1. The effect of mesalazine and ACD on TNBS-induced ulcerative colitis (UC) rats [Note: Blank represents normal rats; Model represents UC model rats; Mesalazine represents UC model rats fed with mesalazine (0.42 g/kg); ACD-L represents UC model rats fed with low dose of ACD (3.97 g/kg); ACD-H represents UC model rats fed with high dose of ACD (19.85 g/kg)]

3.2. Overview of proteomic data and screening of DEPs

A total of 1,182 proteins were identified in five groups of samples, of which 786 proteins were quantified. All the proteins were annotated by Gene Ontology, KEGG, COG, as well as subcellular localization and domain composition analyses (**Supplementary Table 1**). The analysis revealed the changes between Model, Blank, Mesalazine, ACD-L, and ACD-H. The distributions of mass error were close to zero, and most were less than 4 ppm, indicating the high accuracy of modified peptide data obtained by MS (**Figure 2A**). The length of peptide after enzymatic hydrolysis was mainly distributed between 7-15, suggesting that the efficiency of enzymatic hydrolysis is high (**Figure 2B**). The distribution of peptides between Blank and Model groups was narrow, and most of them were within one-fold change (**Figure 2C**). Pearson correlation analysis showed a high correlation between the three biological repeats, thus proving the reliability of our scheme (**Figure 2D**).

There were 372 DEPs between Model and Blank, of which 198 were upregulated and 174 were downregulated. There were 320 proteins with significant differences between Mesalazine and Model, including 95 upregulated and 225 downregulated, 252 proteins between ACD-L and Model, including 81 upregulated and 171 downregulated, and 243 proteins between ACD-H and Model, including 71 upregulated and 172 downregulated. Compared with Blank group, 320 proteins were changed in Mesalazine group, including 126 upregulated proteins and 194 downregulated proteins; 217 proteins were changed in ACD-L group, of which 85 were upregulated and 132 were downregulated; and 218 proteins

were changed in ACD-H group, of which 62 were upregulated and 156 were downregulated. The DEPs were visualized by mapping the volcano map (**Supplementary Figure 1**).

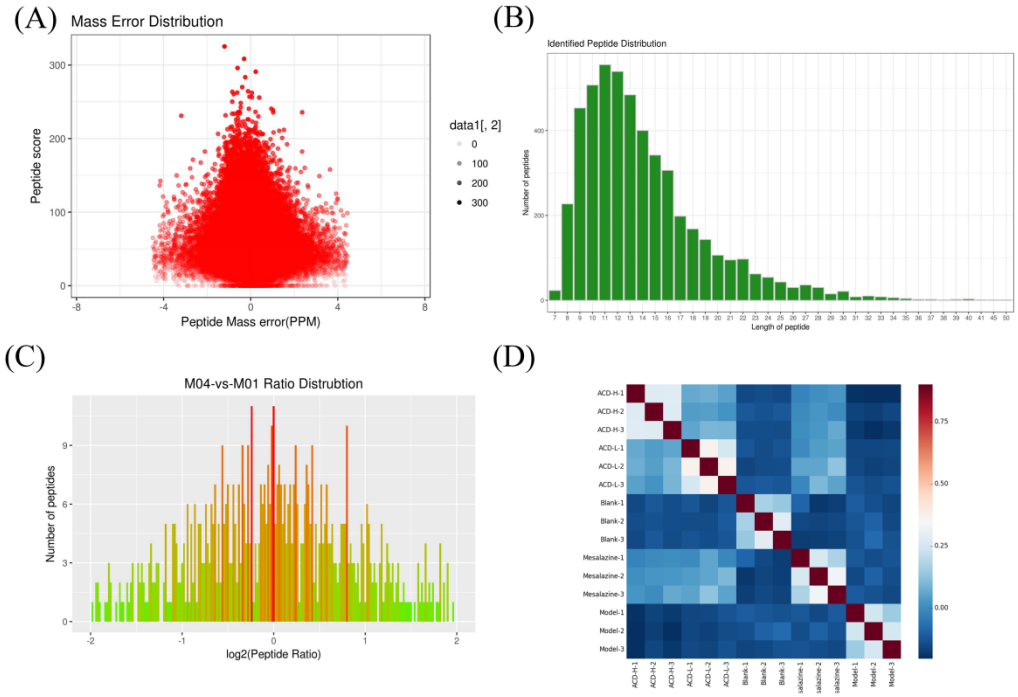

Figure 2. (**A**) The distribution of mass error indicates a high accuracy of modified peptide data obtained from MS; (**B**) The distribution of peptide length indicated high enzymatic efficiency; (**C**) The distribution of peptide ratios (log2 ratio); (D) Repeatability analysis between three replicates of LC-MS/MS experiments

3.3. Biological information analysis of DEPs

DAVID functional annotation was performed to analyze the identified differentially expressed proteins. The DEPs were categorized into cellular components, biological processes, and molecular functions. GO cellular component analysis revealed that most DEPs regulated by TNBS are associated with the cytoskeletal part, cytoplasmic part, and extracellular region part, which are consistent with reports from other groups on the cellular localization of colon proteins [16]. By contrast, the DEPs regulated by ACD-H are mostly associated with plasma membrane, apical plasma membrane, cell periphery, and extracellular region; the DEPs regulated by ACD-L are mostly associated with the extracellular region and extracellular exosome; the DEPs regulated by mesalazine are similar to ACD (**Supplementary Figure 2A**–**D**, **Supplementary Table 2**). GO biological processes analysis revealed that the DEPs regulated by TNBS are mostly involved in the establishment of protein localization to plasma membrane, protein localization to cell periphery, response to epidermal growth factor, and regulation of cell shape. However, the DEPs regulated by ACD-H are mostly associated with response to inorganic substance, wounding, and stimulus, whereas the DEPs regulated by ACD-L are involved in cell migration, regulation of locomotion, and cell motility (**Supplementary Figure 2E**–**H**, **Supplementary Table 3**). GO molecular function analysis linked the DEPs regulated by TNBS to 64 molecular functions, including actin filament binding, catalytic activity, hydro-lyase activity, and galactosidase activity. By comparison, the DEPs regulated by ACD-L are linked to 43 molecular functions, including oxidoreductase activity, acting on peroxide as acceptor, peroxidase activity, peptidase activity, and threonine-type peptidase activity, whereas the DEPs regulated by ACD-H are linked to 64 molecular functions, the most significant of which are metallopeptidase activity, antigen binding, peptidase activity, and transition metal ion binding; the DEPs regulated by mesalazine are related

to 43 molecular functions, including antigen binding and calcium ion binding (**Figure 3**, **Supplementary Table 4**).

We sought to determine which pathways are associated with the identified changes in protein expression in the TNBS model, ACD-L treated rats, and ACD-H treated rats. The DEPs in the TNBS model, ACD-L group, and ACD-H group were significantly enriched in 21, 8, and 7 established KEGG pathways, respectively (**Supplementary Figure 3** and **Supplementary Table 5**). The metabolism of xenobiology by cytochrome P450 and APK signaling pathway are the most important pathways associated with TNBS-mediated colitis.

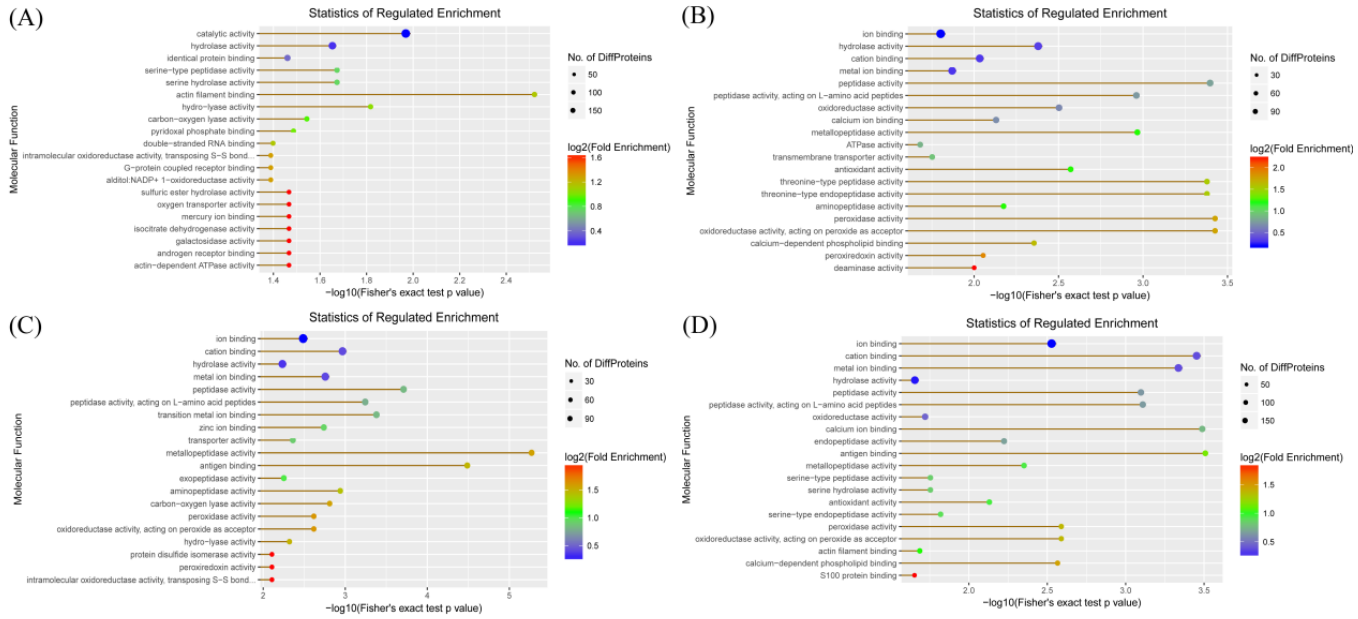

Figure 3. Visualization of significantly enriched GO terms of GO function enrichment of DEPs in (A) Model-vs-Blank, (B) ACD-L-vs-Model, (C) ACD-H-vs-Model, and (D) Mesalazine-vs-Model groups (Note: No. of DiffProteins refers to the number of DEPs enriched in GO terms; the GO enriched fold is shown at the log2 scale in color gradient)

Compared with normal rats, the mesalazine treatment group upregulated complex and coagulation cascades and downregulated TNF signaling pathway, MAPK signaling pathway, and AMPK signaling pathway. In the ACD-L group, staphylococcus aureus infection was upregulated, while Alzheimer's disease and measures were downregulated. In the ACD-H group, the proteins involved in protein, carbohydrate, and fat digestion and absorption were upregulated but those participating in the TGF-β signaling pathway and hepatitis C pathway decreased (**Supplementary Figure 4**).

In order to better compare the information of changed proteins in several groups, cluster analysis was carried out. For upregulated proteins, the most abundant GO terms are antigen binding, peptidase activity, peptidase activity, acting on L-amino acid peptides, and hydrolase activity (**Figure 4**). They have higher enrichment multiples. For down regulated proteins, the most abundant GO terms are ATPase activity, nucleoside triphosphatase activity, hydrolase activity, acting on acid anhydrides, and actin filament binding (**Figure 5**).

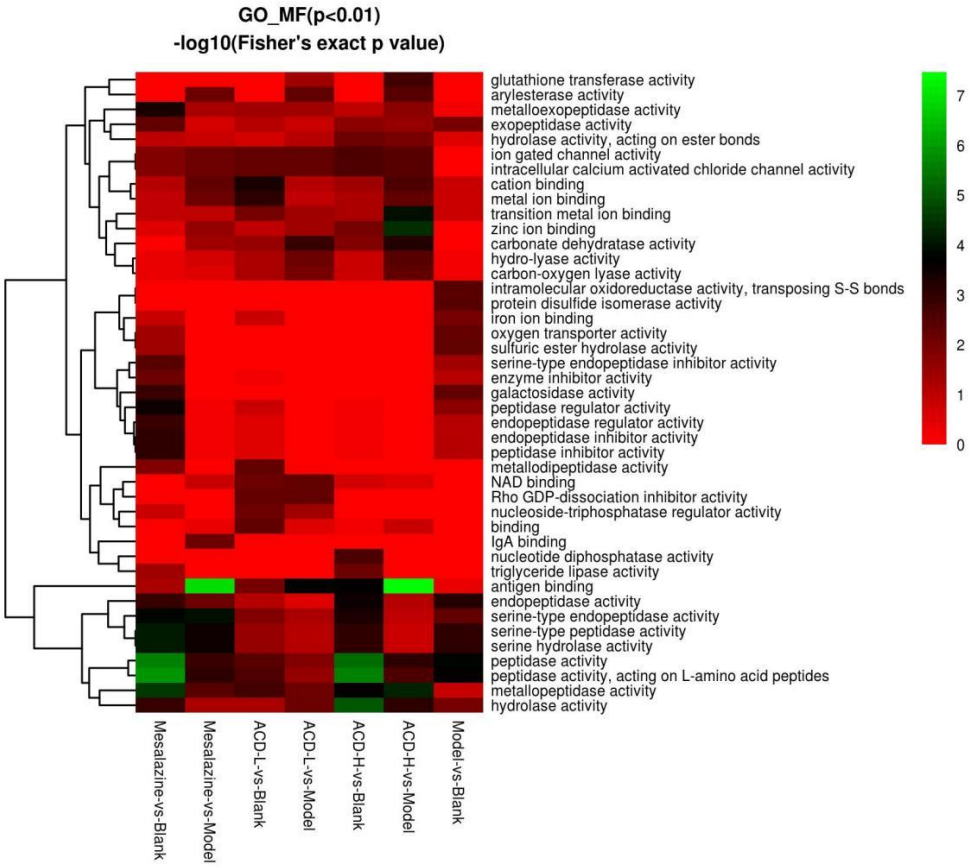

Figure 4. Significantly upregulated GO molecular function cluster in rats in response to different drug treatments

The upregulated proteins in the molecular function category according to Fisher's exact test: peptidase activity and peptidase activity, acting on L-amino acid peptides were upregulated by comparing Mesalazine-vs-Blank; antigen binding was upregulated by comparing Mesalazine-vs-Blank and ACD-H-vs-Model; peptidase activity, peptidase activity, acting on L-amino acid peptides, and hydrolase activity were upregulated by comparing ACD-H-vs-Blank.

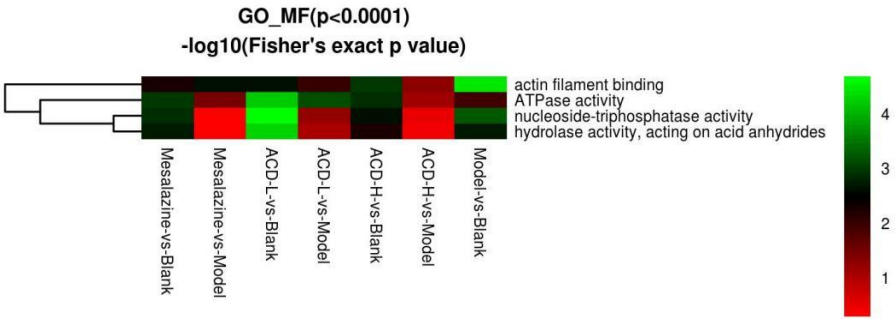

Figure 5. Significantly downregulated GO molecular function cluster in rats in response to different drug treatments

The downregulated proteins in the molecular function category according to Fisher's exact test: ATPase activity, nucleoside triphosphatase activity, and hydrolase activity, acting on acid anhydrides were downregulated by comparing ACD-L-vs-Blank; actin filament binding and nucleoside-triphosphatase activity were downregulated by comparing Model-vs-Blank. The scale bar represents the value calculated by -log 10 (Fisher's exact *p* value) and is distinguished by color. The higher the value, the greener; the smaller the value, the redder it is. Fisher's exact *p* value was used to measure statistical significance.

3.4. Validation of proteomics data by parallel reaction monitoring

In order to validate the accuracy and reproducibility of the proteomics results, PRM analyses were performed, in which eleven proteins were selected as those that may play important roles in drug treatment, and the differentially expressed levels of these proteins were quantified in A, E, K, and M. All the proteins were quantified, and the trend was the same as that of label free. The results of PRM are shown in **Supplementary Table 6** and **Figure 6**. KRT8, HSP90B1, CORO1A, PLEC, MYH11, FLNA, MYH14, LMNA, and LSP1 were all downregulated, whereas FGG and IGHM were upregulated. Fibrinogen gamma chain, type II cytoskeletal 8, myosin-11, and myosin heavy chain 14 are all related to cytoskeleton proteins, immunoglobin heavy constant mu, lamin A, isoform CRA_b, lymphocyte-specific protein 1, and isoform CRA_a, which are related to cellular immunity.

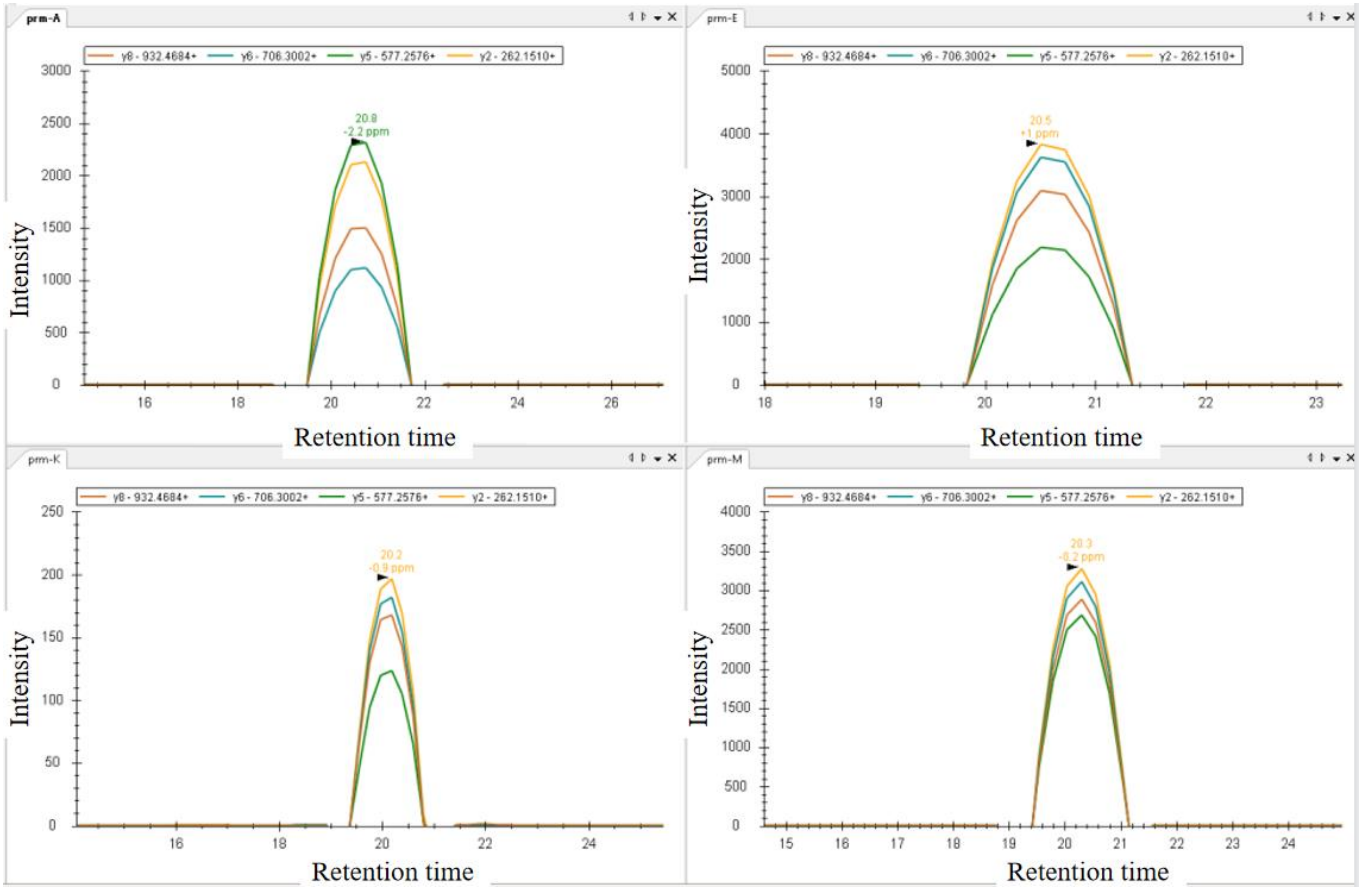

Figure 6. Graphs displaying chromatograms of fragment ions extracted from the peptide KLLEGEESR (PRM for the abundance of fibrinogen gamma chain; the mass measurement error and retention time of the most intense transition are annotated above the peak)

4. Discussion

The use of proteomics to identify key proteins involved in UC rats provides insights into the mechanism of action in the treatment of UC. In this study, 372 DEPs proteins were found in UC rats using label-free technique, and GO enrichment analysis showed significant changes in cytoskeletal proteins in UC rats compared to normal rats. Cytoskeleton plays an important role in regulating various cellular processes related to proliferation, contact inhibition, and anchoring, in addition to cell growth arrest and apoptosis [17]. Studies have shown that cytoskeleton is related to the progression of UC to developing cancer [18]. This is reasonable because UC rats will have obvious histological damage, including necrosis and abscission of some mucosal epithelial cells [19]. In addition, cytochrome P450s (CYPs) also changed in UC rats. CYPs

are a superfamily of the integral membrane, heme-thiolate proteins, entailed in the synthesis and breakdown of various molecules and chemicals within cells [20]. It is a widely accepted hypothesis that UC is caused by a reactive xenobiotic metabolite, which is conjugated before excretion. The imbalance of CYPs will lead to the release of these metabolites, destroy the colonic epithelial barrier, and expose the mucosal immune system to the contents of the lumen, resulting in an inflammatory response [21].

Traditional Chinese medicine (TCM) has a long history in the treatment of UC. For example, the mechanism of luteolin [22], baicalin [23], and cardamonin [24] in the treatment of UC has been partially reported. However, there are only a few reports about ACD. In this study, mesalazine was used as a comparison to elucidate the differences and similarities between traditional herbal medicine and western medicine. The results from the analysis based on GO_BP enrichment showed that the antioxidant activity of UC rats treated with mesalazine and ACD changed. A study reported that mesalazine is effective in reducing tissue damage, oxidative damage, and inflammatory damage, restoring antioxidant capacity, as well as increasing anal sphincter pressure, possibly due to its antioxidant effect [25], which is consistent with our results. Similar studies have been reported on the use of traditional plants, such as Copaifera malmei harms leaves, in reducing micro and macro intestinal injury as well as promoting colonic antioxidation in UC rats [26]. The downregulated proteins in the three treatment groups are involved in many reactions associated with apoptosis and inflammation, suggesting that they may play a role in preventing diseases in healthy rats. The clustering results of GO_MF showed that the antigen binding protein significantly increased in UC rats treated with mesalazine and ACD. UC is an autoimmune disease, and patients with UC have high levels of human leukocyte antigen [27]. Therefore, mesalazine and ACD may be useful to treat UC by regulating the activity of antigen. ACD, unlike mesalazine, downregulated the proteins involved in ATPase activity, which catalyze the hydrolysis of ATP to form ADP and inorganic phosphorus, while also releasing a significant amount of energy. Studies have shown that the level of ATP in patients with UC is lower than that in normal people [28]. The results of this study imply that by limiting ATP breakdown, ACD may revert to normal levels of content.

In order to further explore the molecules of ACD that regulate UC, we compared with previous reports. HSP90B1 [29], Cathepsin D [30], LSP1 [31], S100-A8 [18], and S100-A9 [18] have been reported to be upregulated in UC. In this study, they were enriched by 1.80-, 3.18-, 1.22-, 679.66-, and 20.8-fold in UC rats. These could be the biomarker candidates of UC. Compared with UC rats, HSP90B1 and Cathepsin D were downregulated by 0.77-fold and 0.50-fold in the Mesalazine group, 0.31-fold and 0.69-fold in the ACD-L group, and 0.19-fold and 0.35-fold in the ACD-H group. S100-A8 and S100-A9 were downregulated by 0.04-fold and 0.03-fold in the Mesalazine group, and 0.001-fold and 0.29-fold in the ACD-L group. This shows that mesalazine and ACD may inhibit the expression of HSP90B1, Cathepsin D, S100-A8, and S100-A9 in UC rats. LSP1 was downregulated by 0.34-fold in the Mesalazine group, which may be a special protein comparing to ACD for its treatment in UC rats. Mesalazine's mechanism of action in UC is still unclear. The mechanism of action of mesalazine is via the inhibition of IL-2 production in peripheral mononuclear cells, and thereby inhibiting T-cell proliferation, and interfering with macrophages and neutrophils. Mesalazine may decrease IL-1 and TNF, induce the apoptosis of lymphocytes, and regulate NF-kB. It may also be related to the increase of transcription factor PPAR-γ [4]. Immunohistochemistry analysis showed that the treatment using mesalazine is associated with the decrease of iNOS and NF-KB [25]. In addition, the results of metabolomics and lipidomics showed that the mechanism of mesalazine is related to glycerophospholipid metabolism, pyrimidine metabolism, linoleic acid metabolism, and arginine biosynthesis [19]. The five proteins reported in this study – HSP90B1, Cathepsin D, S100-A8, S100-A9, and LSP1 – have not been reported in previous studies, which might represent potential therapeutic targets for mesalazine.

In addition, a study has shown that RAS superfamily was 2.48-fold and 5.08-fold enriched in cancer and non-cancer tissues of UC patients, respectively [18]. The pathways involved by RAS superfamily include the MAPK signaling pathway, chemokine signaling pathway, focal adhesion pathway, VEGF signaling, and RAS signaling pathway. These pathways are related to tumor initiation and cell transformation [32]. The RAS superfamily includes more than 100 proteins. Among them, RAD23B, which is related to macromolecular catabolism, was upregulated 1.65-fold in UC rats, indicating that UC affects the macromolecular catabolism of rat cells. In the ACD-L, ACD-H, and Mesalazine groups, it was reduced by 0.3469, 0.5586, and 0.0486 times, respectively, indicating that the use of drugs restored the metabolic process to normal. The downstream proteins MAPK1 and MAPK3 of RAS were significantly downregulated by 0.68-fold and 0.41-fold, respectively, in UC rats, while RAC2 was upregulated by 1.37-fold. MAPK1 and MAPK3 are involved in the inhibitor of DNA binding (ID) pathway. The aberrant expression of ID protein is found in many primary tumors and is found to regulate many steps in cancer progression, including neo-angiogenesis, invasion and migration, proliferation and growth, cell-cell interaction, as well as differentiation. RAC2 is involved in the regulation of actin cytoskeleton. This indicates that the treatment process of UC is related to the ID signaling pathway and the upregulation of actin-cytoskeleton pathway, which is consistent with the results of the enrichment analysis.

According to the PRM results, KRT8, MYH11, FLNA, and LMNA are all considered biomarkers of UC. Studies have shown that KRT8 mutation is associated with impaired keratin assembly, which reduces the mechanical elasticity in vivo, thus resulting in intestinal epithelial fragility [31]. However, KRT8 protein is rarely reported in UC. Hence, FGG may be the target protein of mesalazine in the treatment of UC, while KRT8 may be the target protein of ACD.

5. Conclusion

In this paper, the rat UC model was induced by TNBS and tested by HE staining. The results showed that there was a small amount of inflammatory cell infiltration in the submucosa of UC rats. The symptoms experienced by ACD and mesalazine treatment groups improved significantly. The label-free results showed that cytoskeleton and cytochrome P450-related proteins in the colon of UC rats changed, and there was a downregulation of APK signaling pathway. In the treatment of UC with mesalazine and ACD, the antigen binding proteins and antioxidant-related proteins changed, and the pathways related to apoptosis and inflammation were downregulated under the two therapies. The difference is that ACD also downregulated the activity of proteins involved in ATPase activity. SP90B1, Cathepsin D, S100-A8, and S100-A9 may be the therapeutic targets of ACD and mesalazine. The PRM results showed that KRT8, MYH11, FLNA, and LMNA may be biomarkers of UC; the upregulation of KRT8 is largely involved in the mechanism of ACD, and the upregulation of FGG is largely involved in the mechanism of mesalazine. The results demonstrated the similarities and differences between mesalazine and ACD. In this study, LFQ was combined with PRM to reveal the mechanism of TCM for the first time, providing a reference for the development and utilization of TCM in the future.

Funding

National Natural Science Foundation of China (Grant Number: 81860849)

Disclosure statement

The authors declare no conflict of interest.

References

[1] Hindryckx P, Jairath V, Haens GD, 2016, Acute Severe Ulcerative Colitis: From Pathophysiology to Clinical Management. Nature Reviews Gastroenterology & Hepatology, 13(11): 654.

[2] Khare V, Krnjic A, Frick A, et al., 2019, Mesalamine and Azathioprine Modulate Junctional Complexes and Restore Epithelial Barrier Function in Intestinal Inflammation. Scientific Reports, 9(1): 2842.

[3] Kobayashi T, Siegmund B, Le Berre C, et al., 2020, Ulcerative Colitis. Nature Reviews Disease Primers, 6(1): 74.

[4] Ham M, Moss AC, 2014, Mesalamine in the Treatment and Maintenance of Remission of Ulcerative Colitis. Expert Review of Clinical Pharmacology, 5(2): 113-123.

[5] Chao S-Y, Ye S-J, Wang W-W, et al., 2019, Progress in Active Compounds Effective on Ulcerative Colitis from Chinese Medicines. Chinese Journal of Natural Medicines, 2019(2): 81-102.

[6] Xiao Z, Sun P, 2009, Proceedings of the 13th National Anorectal Academic Exchange Conference of Traditional Chinese Medicine, October 16 to 18, 2009: Clinical Observation and Electron Microscopic Study of Anchang Capsule in the Treatment of Ulcerative Colitis. Shaanxi Traditional Chinese Medicine Publisher, Xi'an, Shaanxi, China, 8.

[7] Xiao Z, He Y, Lv Xi, et al., 1993, Self-Made Anchang Decoction in the Treatment of 50 Cases of Ulcerative Colitis. Guangxi Traditional Chinese Medicine, 1993(03): 3-6.

[8] Sun P, 2017, Intestinal Microecological Changes in Rats with Ulcerative Colitis and the Intervention Mechanism of Anchang Decoction. Guangxi Medical University, Guangxi. https://doi.org/10.7666/d.Y3246157

[9] Liang Y, Sun P, 2021, Effect of Anchang Decoction on Inflammation and Immunity in Rats with Ulcerative Colitis Based on miRNA-146a/JAK/STAT/SOCS-3 Signal Pathway. Chinese Journal of Experimental Traditional Medical Formulae, 2021(24): 30-38.

[10] Liu B, Zheng X, Li J, et al., 2021, Revealing Mechanism of Caulis Sargentodoxae for the Treatment of Ulcerative Colitis Based on Network Pharmacology Approach. Bioscience Reports, 41(1): BSR20204005.

[11] Zhang X, Choi FFK, Zhou Y, et al., 2012, Metabolite Profiling of Plasma and Urine from Rats with TNBS-Induced Acute Colitis Using UPLC-ESI-QTOF-MS-Based Metabonomics – A Pilot Study. Febs Journal, 279(13): 2322-2338.

[12] Wang Y, Chen H, Guo Z, et al., 2017, Quantitative Proteomic Analysis of Iron-Regulated Outer Membrane Proteins in Aeromonas Hydrophila as Potential Vaccine Candidates. Fish Shellfish Immun, 68: 1-9.

[13] Huang DW, Sherman BT, Lempicki RA, 2009, Systematic and Integrative Analysis of Large Gene Lists Using DAVID Bioinformatics Resources. Nature Protocols, 4(1): 44.

[14] Roy SM, Becker CH, 2003, Quantification of Proteins and Metabolites by Mass Spectrometry Without Isotopic Labeling or Spiked Standards. Analytical Chemistry, 75(18): 4818-4826.

[15] MacLean B, Tomazela DM, Shulman N, et al., 2010, Skyline: An Open Source Document Editor for Creating and Analyzing Targeted Proteomics Experiments. Bioinformatics, 26(7): 966-968.

[16] Li Y-H, Sun W, Zhou B-J, 2019, iTRAQ-Based Pharmacoproteomics Reveals Potential Targets of Berberine, A Promising Therapy for Ulcerative Colitis. European Journal of Pharmacology, 850: 167-179.

[17] Pawlak G, Helfman D, 2001, Cytoskeletal Changes in Cell Transformation and Tumorigenesis. Current Opinion in Genetics & Development, 11(1): 41-47.

[18] May D, Pan S, Crispin DA, et al., 2011, Investigating Neoplastic Progression of Ulcerative Colitis with Label-Free Comparative Proteomics. Journal of Proteome Research, 10(1): 200-209.

[19] Liu K, Jia B, Zhou L, et al., 2021, Ultraperformance Liquid Chromatography Coupled with Quadrupole Time-of-Flight Mass Spectrometry-Based Metabolomics and Lipidomics Identify Biomarkers for Efficacy Evaluation of Mesalazine in a Dextran Sulfate Sodium-Induced Ulcerative Colitis Mouse Model. Journal of Proteome Research, 20(2): 1371-1381.

[20] Montellano P, 2010, Hydrocarbon Hydroxylation by Cytochrome P450 Enzymes. Chemical Reviews, 110(2): 932-48.

[21] Sen A, Stark H, 2019, Role of Cytochrome P450 Polymorphisms and Functions in Development of Ulcerative Colitis. World Journal of Gastroenterology, 25(23): 2846-2862.

[22] Ganapasam S, Pandurangan AK, Kumar S, et al., 2014, Luteolin, a Bioflavonoid Inhibits Azoxymethane-Induced Colon Carcinogenesis: Involvement of iNOS and COX-2. Pharmacognosy Magazine, 10(38): 306-10.

[23] Zhang CL, Zhang S, He WX, et al., 2017, Baicalin May Alleviate Inflammatory Infiltration in Dextran Sodium Sulfate-Induced Chronic Ulcerative Colitis Via Inhibiting IL-33 Expression. Life Sciences, 186: 125-132.

[24] Kim YJ, Ko H, Park JS, et al., 2010, Dimethyl Cardamonin Inhibits Lipopolysaccharide-Induced Inflammatory Factors Through Blocking NF-KappaB P65 Activation. International Immunopharmacology, 10(9): 1127-1134.

[25] Owens DW, Wilson NJ, Hill AJM, et al., 2004, Human Keratin 8 Mutations That Disturb Filament Assembly Observed in Inflammatory Bowel Disease Patients. Journal of Cell Science, 117(Pt 10): 1989-1999.

[26] Pavan E, Damazo AS, Arunachalam K, et al., 2020, Copaifera Malmei Harms Leaves Infusion Attenuates TNBS-Ulcerative Colitis Through Modulation of Cytokines, Oxidative Stress and Mucus in Experimental Rats. Journal of Ethnopharmacology, 267: 113499.

[27] Gleeson MH, Walker JS, Wentzel J, et al., 1972, Human Leucocyte Antigens in Crohn's Disease and Ulcerative Colitis. Gut, 13(6): 438-440.

[28] Kameyama JI, Narui H, Inui M, et al., 1984, Energy Level in Large Intestinal Mucosa in Patients with Ulcerative Colitis. Tohoku Journal of Experimental Medicine, 143(2): 253.

[29] Bellmann K, 2000, p38-dependent Enhancement of Cytokine-induced Nitric-oxide Synthase Gene Expression by Heat Shock Protein 70. Journal of Biological Chemistry, 275(24): 18172-18179.

[30] Urbanelli L, Emiliani C, Massini C, et al., 2008, Cathepsin D Expression Is Decreased in Alzheimer's Disease Fibroblasts. Neurobiology of Aging, 29(1): 12-22.

[31] Zarubin T, Han J, 2005, Activation and Signaling of the p38 MAP Kinase Pathway. Cell Research, 15(1): 11-18.

[32] Goldfinger LE, 2008, Choose your Own Path: Specificity in Ras GTPase Signaling. Molecular Biosystems, 2008(4): 293-299.